Indian J. Phys. **76B** (3), 289-296 (2002)

I J P B
an international journal

Thermal and mass diffusion on unsteady hydromagnetic flow with heat flux and accelerated boundary motion

M Acharya*[1], G C Dash[2] and L P Singh[3]

[1]Department of Physics, College of Basic Science & Humanities, O U A T, Bhubaneswar-751 003, Orissa, India

[2]Department of Mathematics, C E T, O U A T, Bhubaneswar-751 003, Orissa, India

[3]Department of Physics, Utkal University, Bhubaneswar-751 004, Orissa, India

Received 19 July 2001, accepted 22 April 2002

Abstract This paper concerns with the effect of thermal and mass diffusion on unsteady free convection flow of an incompressible and electrically conducting fluid subjected to constant heat flux and accelerated boundary motion in presence of constant magnetic field. An exact solution has been obtained for species concentration, temperature and velocity variables. The fluid velocity and skin friction have been computed for some saturated liquids. The results are discussed with respect to buoyancy ratio parameter (N) and Hartmann number (m).

Keywords Thermal and mass diffusion, unsteady hydromagnetic flow, exact solution

PACS Nos. 47.15.Cb, 47.65.+a, 44.30.+v

1. Introduction

Magnetohydrodynamics is currently undergoing a period of great enlargement and differentiation of subject matter. The MHD mass transfer process are important in power engineering, chemistry and metallurgy. Many studies of such proceses have been concerned solely with thermal convection even though buoyancy effects resulting from concentration differences can be just as important in generating fluid motion as temperature gradients [1,2]. The buoyancy effects due to mass diffusion for steady state and pure convection condition have already been studied by several workers [3-8]. The effect of Hall Current on the unsteady free convection flow of a viscous incompressible and electrically conducting fluid with mass transfer, has been reported by Hossain and Rashid [9]. Later on, Hall Current on the unsteady hydromagnetic flow with simultaneous thermal and mass diffusion was studied by Acharya *et al* [10]. Free convection fluid flows with heat flux are encountered in many industrial problem such as nuclear reactor, solar energy collectors *etc*. The effect of magnetic field, gravitational forces on the flow characteristics of an electrically conducting fluid have been an active area of research in geophysics. Recently, unsteady hydromagnetic free convection flow with heat flux and accelerated boundary motion was studied by Chandran *et al* [11]. Callahan and Marner [12] have analysed transient, laminar, free convection over a vertical plate with buoyancy effect. Garg [13] has studied transient laminar, combined free and forced convection over an isothermal vertical plate subjected to a step change in temperature and concentration.

In the present paper, we have obtained an exact solution for the unsteady free convection with thermal and mass diffusion of an electrically conducting fluid past an infinite vertical plate subjected to uniformely accelerated motion and constant heat flux. An external magnetic field of strength B_0 is applied perpendicular to the plate. Under the condition that the magnetic Reynold number is small, the induced magnetic field is negligible compared with the applied field. This condition is usually well satisfied in flow velocity free convection [14].

*Corresponding Author

Most of the studies cited above reported less cumbersome governing equations which could be subjected to analytical solution procedures. However, the availability of closed form solutions is still dependent on the nature of the boundary value problem considered. If the boundary conditions are prescribed in terms of variable quantities, the solution procedure are generally more tedious. The present analysis deals with the accelerated motion of the plate considering a variable boundary value problem in terms of time variable. An exact solution to this problem has been derived by using Laplace transforms.

2. Formulation of the problem

The physical configuration consists of unsteady flow of an electrically conducting and incompressible viscous fluid with simultaneous heat and mass transfer along an infinite vertical nonconducting palate. The x' axis is taken along with wall in the horizontal direction and y' axis perpendicular to the plate into the fluid. A uniform magnetic field B_0 is applied in the y' direction. Initially, the plate and fluid are at rest and at some temperature T'_∞. Now the plate is set into sudden acceleration with velocity Ut' in x' direction, where t' is the time variable and U is a constant. Heat is also supplied to the plate at constant rate. We assume that (1) molecular transport properties are constant, (2) density variation due to temperature and concentration difference is approximated by Boussinesq approximation, (3) mass fraction of diffusing species is low compared to that of other species in the binary mixture, (4) viscous dissipation in the energy equation is negligible, (5) no chemical reaction takes place in the fluid during the flow. As the plate is of infinite length, all variables in this problem are functions of y' and t'. According to Rayleigh, convective terms and pressure gradient term in momentum and energy equations are neglected. Hence with usual boundary layer approximation, the basic equations are expressed in the following form

$$\frac{\partial u'}{\partial t'} = \nu \frac{\partial^2 u'}{\partial y'^2} + g\beta(T' - T'_\infty) + g\beta^*(C' - C'_\infty) - \frac{\sigma B_0^2 u'}{\rho} \tag{1}$$

$$\frac{\partial T'}{\partial t'} = \frac{k}{\rho c_p} \frac{\partial^2 T'}{\partial y'^2}, \tag{2}$$

$$\frac{\partial C'}{\partial t'} = D \frac{\partial^2 C'}{\partial y'^2}, \tag{3}$$

where u' is the velocity in the x' direction. T' is the temperature of the fluid. C' is the species concentration, k is the thermal conductivity, D is the molecular diffusivity, g the acceleration due to gravity, β the volumetric coefficient of thermal expansion, β^* the volumetric coefficient of expansion with concentration, ν the kinematic viscosity, ρ the density, σ the electrical conductivity and C_p the specific heat of fluid at constant pressure. The initial and boundary conditions relevant to the problem are

$$u' = 0,\ T' = T'_\infty,\ C' = C'_\infty, \quad \text{for } y' \geq 0 \text{ and } t' \leq 0,$$

$$u' = Ut', \ -\frac{\partial T'}{\partial y'} = \frac{q_w}{k}, \ -\frac{\partial C'}{\partial y'} = \frac{m_w}{D}, \quad \text{at } y' = 0 \text{ for } t' > 0,$$

$$u' \to 0,\ T' \to T'_\infty,\ C' \to C'_\infty \quad \text{as } y' \to \infty \text{ for } t' > 0, \tag{4}$$

where q_w is the constant heat flux per unit area and m_w is the constant mass flux per unit area. Let us introduce the following non-dimensional quantities

$$y = y'(U/\nu^2)^{1/3},\ t = t'(U^2/\nu)^{1/3},\ u = u'/(\nu U)^{1/3},$$

$$T = kU^{1/3}(T' - T'_\infty)/(q_w \nu^{2/3}),$$

$$C = DU^{1/3}(C' - C'_\infty)/(m_w \nu^{2/3}),$$

$$Pr = \nu \rho c_p / k,\ Sc = \nu / D,$$

$$Gr = \nu^{2/3} q_w g\beta / (kU^{4/3}),$$

$$Gc = \nu^{2/3} m_w g\beta^* / (DU^{4/3}),$$

$$m = \sigma B_0^2 \nu^{1/3} / (\rho U^{2/3}).$$

eqs. (1), (2) and (3) can be rewritten in the form :

$$\frac{\partial u}{\partial t} = \frac{\partial^2 u}{\partial y^2} + GrT + GcC - mu, \tag{5}$$

$$\frac{\partial T}{\partial t} = \frac{1}{Pr} \frac{\partial^2 T}{\partial y^2}, \tag{6}$$

$$\frac{\partial C}{\partial t} = \frac{1}{Sc} \frac{\partial^2 C}{\partial y^2}. \tag{7}$$

The corresponding initial and boundary conditions are as follows :

$$u = 0,\ T = 0,\ C = 0, \quad \text{for } y \geq 0 \text{ and } t \leq 0,$$

$$u = t, \ -\frac{\partial T}{\partial y} = -1, \ -\frac{\partial C}{\partial y} = -1, \quad \text{at } y = 0 \text{ for } t > 0,$$

$$u \to 0,\ T \to 0,\ C \to 0, \quad \text{as } y \to \infty \text{ for } t > 0. \tag{8}$$

where Pr is the Prandtl number, Sc is the Schmidt number, Gr is the Grashof number for heat transfer, Gc is the Grashof number for mass transfer and m is the square of Hartmann number.

3. Method of solution

The Laplace transform method is used to obtain an exact analytical solution for this time-dependent MHD free convection problem. However, the difficulties arise in obtaining inverse transforms when kernals assume complicated forms. We use convolution integration to overcome this difficulties. Let us introduce the following variables.

$$\bar{u} = \int_0^\infty u \exp(-st)\,dt,$$

$$\bar{\theta} = \int_0^\infty T \exp(-st)\,dt,$$

$$\bar{C} = \int_0^\infty C \exp(-st)\,dt. \tag{9}$$

Now eqs. (5), (6) and (7) are transformed into

$$\frac{d^2\bar{u}}{dy^2} - (m+s)\bar{u} + Gr\,\bar{\theta} + Gc\,\bar{C} = 0, \tag{10}$$

$$\frac{d^2\bar{\theta}}{dy^2} - Pr\,s\bar{\theta} = 0, \tag{11}$$

$$\frac{d^2\bar{C}}{dy^2} - (Sc)s\bar{C} = 0. \tag{12}$$

The new boundary conditions are

$$\bar{u} = \frac{1}{s^2},\ \frac{d\bar{\theta}}{dy} = -\frac{1}{s},\ \frac{d\bar{C}}{dy} = -\frac{1}{s} \quad \text{at } y = 0,$$

$$\bar{u} \to 0,\ \bar{\theta} \to 0,\ \bar{C} \to 0 \quad \text{as } y \to \infty. \tag{13}$$

The solutions of eqs. (10), (11) and (12) can be written as

$$\bar{u} = \frac{1}{s^2}\exp\left[-(m+s)^{1/2}y\right] - \frac{\alpha_1}{(\beta_1+s)s^{3/2}}\left[\exp\left\{-(m+s)^{1/2}y\right\} - \exp\left\{-Pr^{1/2}s^{1/2}\right\}y\right] - \frac{\alpha_2}{(\beta_2+s)s^{3/2}} \times \left[\exp\left\{-(m+s)^{1/2}y\right\} - \exp\left\{-Sc^{1/2}s^{1/2}\right\}y\right], \tag{14}$$

$$\bar{\theta} = \frac{1}{Pr^{1/2}s^{3/2}}\exp\left\{-y(Prs)^{1/2}\right\}, \tag{15}$$

$$\bar{C} = \frac{1}{Pc^{1/2}s^{3/2}}\exp\left\{-y(Sc\,s)^{1/2}\right\}, \tag{16}$$

where $\alpha_1 = \dfrac{Gr}{(1-Pr)Pr^{1/2}}$, $\beta_1 = \dfrac{m}{1-Pr}$,

$$\alpha_2 = \frac{GrN}{(1-Sc)Sc^{1/2}},\quad \beta_2 = \frac{m}{1-Sc},$$

$$N = \frac{\beta^*(m_w/D)}{\beta(q_w/k)}. \tag{17}$$

N is the buoyancy ratio parameter so that $N = 0$ for thermal driven flow and $N \to \infty$ for mass driven flow, positive for both effects combining to drive the flow and negative for effects opposing it [1].

The temperature, species concentration and velocity distribution can be obtained from eqs. (15), (16) and (14) respectively on inversion [15–19].

$$T(y,t) = 2Pr^{-1/2}(t/\pi)^{1/2}\exp\left(\frac{-y^2Pr}{4t}\right) - y\,\mathrm{erfc}\left(\frac{Pr^{1/2}y}{2t^{1/2}}\right), \tag{18}$$

$$C(y,t) = 2Sc^{-1/2}(t/\pi)^{1/2}\exp\left(\frac{-y^2Sc}{4t}\right) - y\,\mathrm{erfc}\left(\frac{Sc^{1/2}y}{2t^{1/2}}\right), \tag{19}$$

$$u(y,t) = u_1(y,t) + u_2(y,t) + u_3(y,t) + u_4(y,t) + u_5(y,t), \tag{20}$$

where

$$u_1(y,t) = \frac{t^{1/2}}{2m^{1/2}}\left[\left\{\frac{y}{2t^{1/2}} + (mt)^{1/2}\right\} \times \exp(m^{1/2}y)\,\mathrm{erfc}\left\{\frac{y}{2t^{1/2}} + (mt)^{1/2}\right\} - \left\{\frac{y}{2t^{1/2}} - (mt)^{1/2}\right\}\exp(-m^{1/2}y) \times \mathrm{erfc}\left\{\frac{y}{2t^{1/2}} - (mt)^{1/2}\right\}\right],$$

$$u_2(y,t) = -\alpha_1\int_0^t V_1(y,x)\,H(t-x)\,dx,$$

$$u_3(y,t) = \alpha_1\int_0^t W_1(y,x)\,H(t-x)\,dx,$$

$$V_1(y,t) = \frac{1}{2}\exp(-\beta_1 t)\left[\exp\left\{-(m-\beta_1)^{1/2}y\right\} \times \mathrm{erfc}\left\{\frac{y}{2t^{1/2}} + (mt-\beta_1 t)^{1/2}\right\}\right],$$

$$W_1(y,t) = \frac{1}{2}\exp(-\beta_1 t)\left[\exp\left(-iPr^{1/2}\beta^{1/2}y\right) \times \mathrm{erfc}\left\{\frac{Pr^{1/2}y}{2t^{1/2}} - i(\beta_1 t)^{1/2}\right\} + \exp\left(i\,\mathrm{Pr}^{1/2}\,\beta_1^{1/2}y\right) \times \mathrm{erfc}\left\{\frac{\mathrm{Pr}^{1/2}\,y}{2t^{1/2}} + i(\beta_1 t)^{1/2}\right\}\right],$$

$$u_4(y,t) = -\alpha_2\int_0^t V_2(y,x)\,H(t-x)\,dx,$$

$$u_5(y,t) = \alpha_2\int_0^t W_2(y,x)\,H(t-x)\,dx,$$

$$V_2(y,t) = \frac{1}{2}\exp(-\beta_2 t)\left[\exp\left\{-(m-\beta_2)^{1/2}y\right\} \times \mathrm{erfc}\left\{\frac{y}{2t^{1/2}} - (m-\beta_2 t)^{1/2}\right\} + \exp\left\{(m-\beta_2)^{1/2}\right\} \times \mathrm{erfc}\left\{\frac{y}{2t^{1/2}} + (mt-\beta_2 t)^{1/2}\right\}\right],$$

$$W_2(y,t)=\frac{1}{2}\exp(-\beta_2 t)\left[\exp\left(-iSc^{1/2}\beta_2^{1/2}y\right)\times\operatorname{erfc}\left\{\frac{Sc^{1/2}y}{2t^{1/2}}-i(\beta_2 t)^{1/2}\right\}+\exp\left(iSc^{1/2}\beta_2^{1/2}y\right)\times\operatorname{erfc}\left\{\frac{Sc^{1/2}y}{2t^{1/2}}+i(\beta_2 t)^{1/2}\right\}\right],$$

$$H(t)=2(t/\pi)^{1/2}. \tag{21}$$

and erfc denotes the complementary error function. Velocity given by eq. (20) involves convolution integrals u_2, u_3, u_4, u_5. However, u_3 and u_5 can be expressed explicitly in terms of exponential and complementary error functions without convolution. We rewrite the corresponding expression *i.e*, 3rd and 5th term of eq. (14) in the (s, y) plane.

$$\frac{\alpha_1}{\beta_1}\left[\exp\left(\frac{-Pr^{1/2}s^{1/2}y}{s^{3/2}}\right)-\exp\left(\frac{-Pr^{1/2}s^{1/2}y}{(\beta_1+s)s^{1/2}}\right)\right], \tag{22}$$

$$\frac{\alpha_2}{\beta_2}\left[\exp\left(\frac{-Sc^{1/2}s^{1/2}y}{s^{3/2}}\right)-\exp\left(\frac{-Sc^{1/2}s^{1/2}y}{(\beta_2+s)s^{1/2}}\right)\right], \tag{23}$$

which on inversion, enables us to write u in the alternate form.

$$u(y,t)=u_1(y,t)+u_2(y,t)+u_{31}(y,t)+u_{32}(y,t)+u_4(y,t)+u_{51}(y,t)+u_{52}(y,t), \tag{24}$$

where u_1, u_2, u_4 are defined in eq. (21)

and $$u_{31}(y,t)=\frac{\alpha_1}{\beta_1}Pr^{1/2}\theta(y,t),$$

$$u_{32}(y,t)=\frac{i\alpha_1}{\beta_1^{3/2}}W_1(y,t),$$

$$u_{51}(y,t)=\frac{\alpha_2}{\beta_2}Sc^{1/2}C(y,t)$$

$$u_{52}(y,t)=\frac{i\alpha_2}{\beta_2^{3/2}}W_2(y,t). \tag{25}$$

The solutions given by eqs. (20) and (24) are equivalent. Therefore, either of them can be used to obtain velocity distribution. Further, the solutions given by eqs. (20) and (24) involve imaginary quantities, when β_1 and β_2 are positive quantities which correspond to Prandtl number and Schmidt number less than unity [$u_{32}(y,t)$ and $u_{52}(y,t)$]. In this case, $W_1(y,t)$ and $W_2(y,t)$ have to be re-expressed in a form suitable for computational purposes. However, results are presented for saturated fluids for which Prandtl number and Schmidt number are greater than unity. For completeness, we write an expression for W_1 and W_2 for positive β_1 and β_2.

$$W_1(y,t)=\exp(-\beta_1 t)\operatorname{Im}\left[\exp\left(iPr^{1/2}\beta_1^{1/2}y\right)\times\operatorname{erfc}\left\{\frac{Pr^{1/2}y}{2t^{1/2}}+i(\beta_1 t)^{1/2}\right\}\right] \tag{26}$$

$$W_2(y,t)=\exp(-\beta_2 t)\operatorname{Im}\left[\left(iSc^{1/2}\beta_2^{1/2}y\right)\times\operatorname{erfc}\left\{\frac{Sc^{1/2}y}{2t^{1/2}}+i(\beta_2 t)^{1/2}\right\}\right] \tag{27}$$

where Im denotes imaginary part. An approximate value for W_1 and W_2 can be obtained using the series approximation for the complementary function [18]

$$\operatorname{erfc}(x+iy)=\operatorname{erfc}x-\frac{\exp(-x^2)}{2\pi x}\times[1-\cos(2xy)+i\sin(2xy)]-\left(\frac{2}{\pi}\right)\exp(-x^2)\sum_{n=1}^{\infty}\frac{\exp(-n^2/4)}{n^2+4x^2}\times[f_n(x,y)+ig_n(x,y)]+\epsilon(x,y), \tag{28}$$

where $f_n(x,y)=2x-2x\cosh(ny)\cos(2xy)+n\sinh(ny)\sin(2xy)$,

$g_n(x,y)=2x\cosh(ny)\sin(2xy)+n\sinh(ny)\cos(2xy)$,

$|\epsilon(x,y)|\simeq|erf(x+iy)|10^{-16}$.

It may be noted that the solution for velocity variable obtained above can be used to find the induced magnetic field $\boldsymbol{B}_x(y,t)$. $\boldsymbol{B}_x$ is given by the following equation

$$-\frac{\partial \boldsymbol{B}_x}{\partial y}=\sigma\boldsymbol{B}_0 u \tag{29}$$

with the boundary conditions

$\boldsymbol{B}_x(y,t)=0$ as $y\to\infty$

and $[\boldsymbol{B}_x]=0$ at the insulator wall ($y=0$) or

$[\boldsymbol{B}_x]=j_z$ (sheet current) at the perfect conductor wall ($y=0$),

where $[\boldsymbol{B}_x]\equiv\boldsymbol{B}_x(+0,t)-\boldsymbol{B}_x(-0,t)$ *i.e.* jump of $\boldsymbol{B}_x$ at the boundary.

We thus obtain $\boldsymbol{B}_x(y,t)=-\sigma\boldsymbol{B}_0\int_{\infty}^{y}u(y,t)\,dy$ both for the insulator and conductor wall for $y>0$ and

$$\boldsymbol{B}_x(y,t)=-\sigma\boldsymbol{B}_0\int_0^{\infty}u(y,t)\,dy$$ for the insulator wall.

$\boldsymbol{B}_x(y,t)=0$ for the perfect conductor wall, (30)

for $y<0$. Also $j_z=\sigma\boldsymbol{B}_0\int_0^{\infty}u(y,t)\,dy$, the sheet current at $y=0$, for the perfect conductor wall.

Now, we calculate important physical parameter skin friction. The skin friction on the boundary is given by

$$\tau = -\left(\frac{\partial u}{\partial y}\right)_{y=0} \tag{31}$$

and using eq. (20), we have

$$\tau = \tau_1 + \tau_2 + \tau_3 + \tau_4 + \tau_5, \tag{32}$$

where $\tau_1 = -\frac{2mt+1}{2m^{1/2}}\left[1 - \text{erfc}(mt)^{1/2} + \left(\frac{t}{\pi}\right)^{1/2} \exp(-mt)\right]$,

$$\tau_2 = \alpha_1 \int_0^t V_1(x)\, H(t-x)dx,$$

$$\tau_3 = -\alpha_1 \int_0^t W_1(x)\, H(t-x)dx,$$

$$\tau_4 = \alpha_2 \int_0^t V_2(x)\, H(t-x)dx,$$

$$\tau_5 = -\alpha_2 \int_0^t W_2(x)\, H(t-x)dx$$

and $V_1(t) = \exp(-\beta_1 t)\left[(m-\beta_1)^{1/2}\{\text{erfc}(mt-\beta_1 t)^{1/2} - 1\} - \exp(\beta_1 t - mt)/(\pi t)^{1/2}\right]$,

$V_2(t) = \exp(-\beta_2 t)\left[(m-\beta_2)^{1/2}\{\text{erfc}(mt-\beta_2 t)^{1/2} - 1\} - \exp(\beta_2 t - mt)/(\pi t)^{1/2}\right]$,

$W_1(t) = \exp(-\beta_1 t)\left[i(Pr\beta_1)^{1/2}\{\text{erfc}(-\beta_1 t)^{1/2} - 1\} - Pr^{1/2}\exp(\beta_1 t)/(\pi t)^{1/2}\right]$,

$W_2(t) = \exp(-\beta_2 t)\left[i(Sc\beta_2)^{1/2}\{\text{erfc}(-\beta_2 t)^{1/2} - 1\} - Sc^{1/2}\exp(\beta_2 t)/(\pi t)^{1/2}\right]$. (33)

If u is given by eq. (24), then τ takes the form

$$\tau = \tau_1 + \tau_2 + \tau_3 + \tau_4 + \tau_n + \tau_{nl},$$

where τ_1, τ_2 and τ_4 are defined earlier.

and $\tau_n = \alpha_1 Pr^{1/2}\left[1 - \exp(-\beta_1 t)\right]/\beta_1$,

$\tau_{nl} = \alpha_2 Sc^{1/2}\left[1 - \exp(-\beta_2 t)\right]/\beta_2$.

The arguments of complementary error functions can assume real and complex values depending on fluid properties. Therefore, the expression for velocity and skin friction can be expressed in terms of real and imaginary parts for numerical calculations. For incompressible fluids, the arguments become real and in this case, error function have been approximated by Abramowitz and Stegun [18] as

$$erf(x) = 1 - \left(\sum_{i=1}^{5} a_i z^i\right)\exp(-x^2) + \epsilon(x), \tag{34}$$

where $z = (1+px)^{-1}$, $p = 0.3275911$,

$a_1 = 0.254829592$, $a_2 = -0.284496736$,

$a_3 = 1.421413741$, $a_4 = -1.453152027$

$a_5 = 1.061405429$, $|\epsilon(x)| \le 1.5 \times 10^{-7}$.

4. Results and discussion

The velocity of free convection fluid flow (eqs. 20 and 24) given in terms of exponential and error functions are themselves functions of space and time variables as well as the dimensionless parameters characterising the problem. We have evaluated the fluid velocity for some typical values of the governing parameters in order to predict their significance in flow evolution. The variation of velocity is shown in the Figures (1–6) and temperature or concentration

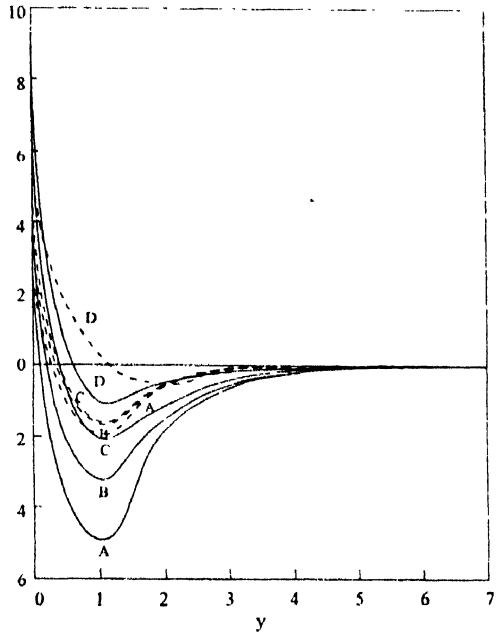

Figure 1. Velocity profiles for $Pr = Sc = 7.0$, $N = -2.0$, $Gr = 1.0$, $m = 1.0$ — and $m = 2.0$ ---- Values of t for curve $A = 0.2$, $B = 0.4$, $C = 0.6$, $D = 0.8$

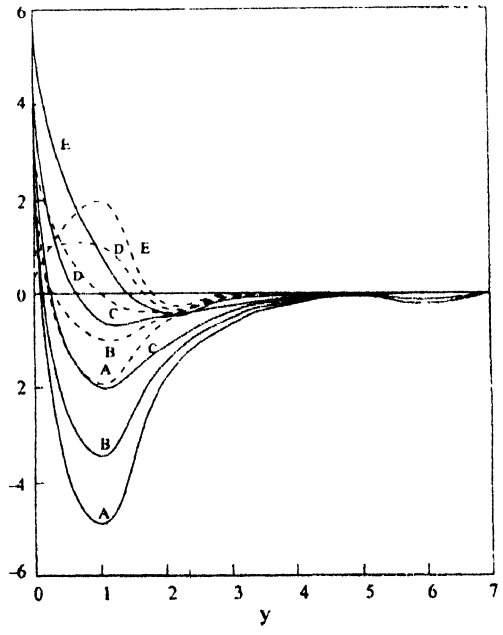

Figure 2. Velocity profiles for $Pr = Sc = 7.0$, $Gr = 1.0$, $t = 0.2$, $m = 1.0$ — and $m = 2.0$ ---- Values of N for curve $A = -2$, $B = -1$, $C = 0$, $D = 1$, $E = 2$.

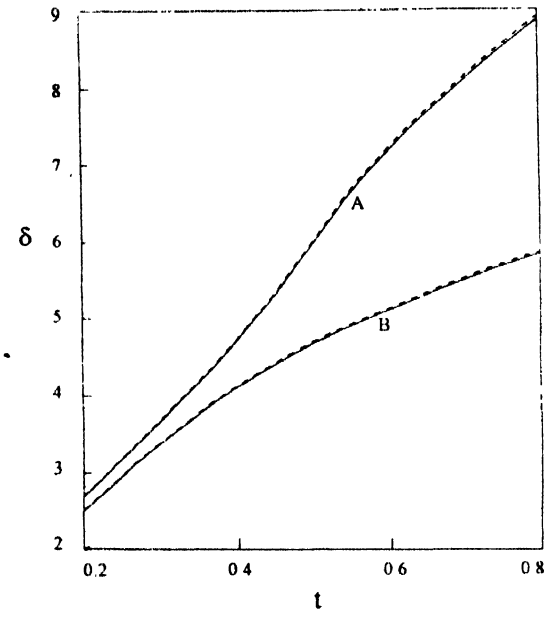

Figure 3. Boundary layer thickness δ $Pr = Sc = 7.0$, $Gr = 1.0$, $N = -2.0$, δ_1 = — and δ_2 = ---- Values of m for curve $A = 1.0$, $B = 2.0$.

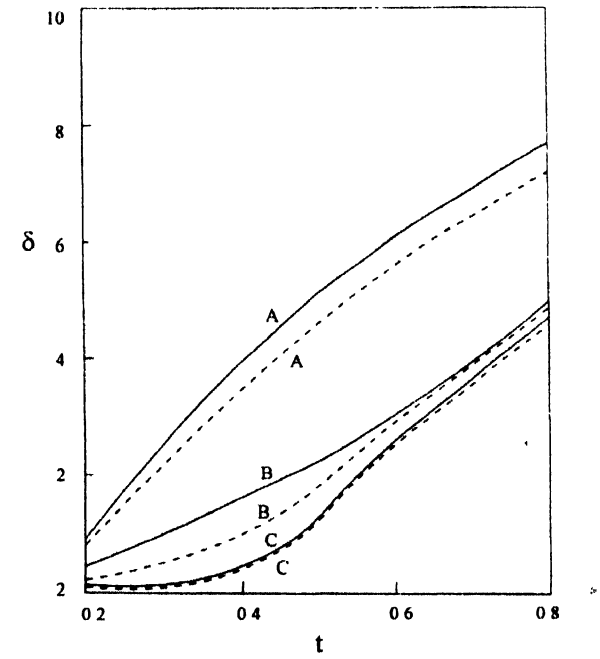

Figure 4. Variation of velocity with time $Pr = Sc = 7.0$, $Gr = 1.0$, $N = 2.0$. Values of y for curve $A = 1.0$, $B = 2.0$, $C = 3.0$, $m = 1.0$— $m = 2.0$ ----.

variations are shown graphically in Figure 7. Tables (1, 2) provide the skin friction at the boundary. The results pertain to two saturated liquids of different viscosities sulphurdioxide (SO_2) and water (H_2O) at a temperature 20°C. The Prandtl number of these liquids have been considered to be 2.0 and 7.0 respectively. Figures 1 and 5 indicate a stronger flow reversal with decreasing Hartmann number in outer boundary region for negative values of N.

The uniformly accelerated motion of bounding plate $y = 0$ for a given value of U is depicted in Figures 1 and 5 for H_2O and SO_2 respectively. An increase in the plate velocity results in proportional increase in the fluid velocity and after attaining the minimum value, fluid velocity steadily reaches to zero in layers of variable depths. The velocity reversal is observed for $N = -2.0$ and $N = -1.0$. These results follow from a very complicated interaction of two buoyancy effects through velocity to the diffusion mechanism Thus, the approach of the boundary layer fluid velocity profile to its free stream value (zero) depends on boundary wall velocity as well as magnetic parameter m for a given value of Grashof numbers and buoyancy ratio parameter

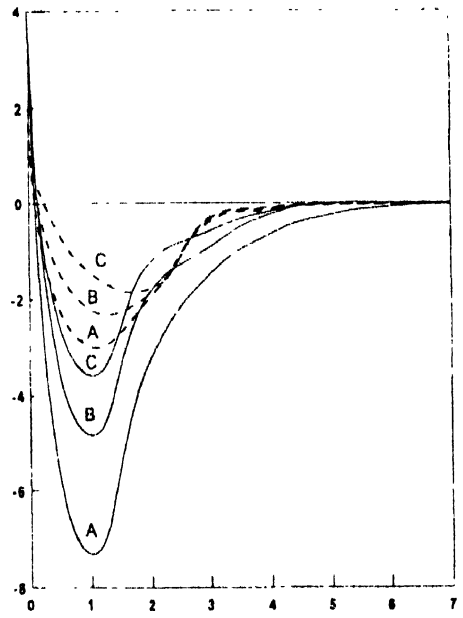

Figure 5. Velocity profiles against y for $Pr = 2.0$, $Sc = 23.53$, $Gr = 1.0$, $N = -1.0$, $m = 1.0$ — —, $m = 2.0$ ---- Values of t for curve $A = 0.2$ $B = 0.4$, $C = 0.6$.

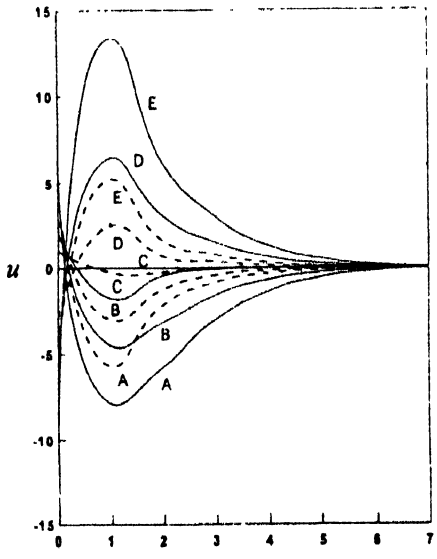

Figure 6. Velocity profiles against y for $Pr = 2.0$, $Sc = 23.53$, $Gr = 1.0$, $t = 0.2$, $m = 1.0$ ——, $m = 2.0$ ----. Values of N for curve $A = -2.0$, $B = -1.0$, $C = 0.0$, $D = 1.0$, $E = 2.0$.

This enables one to look at the effects of these parameters on the boundary layer thickness.

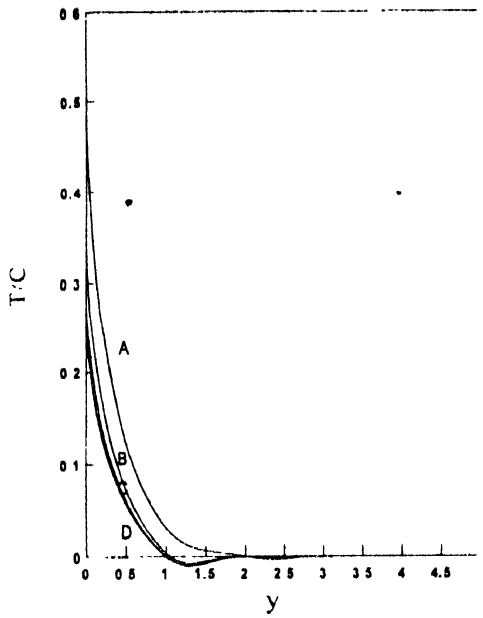

Figure 7. Temperature/concentration profiles as a function of y for various values of Pr/Sc at $t = 0.2$. Values of Pr/Sc for curve $A = 1.0$, $B = 2.0$, $C = 3.0$ and $D = 4.0$

Table 1. Variation of u for $t = 0.4$

Pr	Sc	Gr	N	y	m	u
2.0	23.53	1.0	+1	1.0	1.0	6.50833
					2.0	2.48829
				2.0	1.0	3.03864
					2.0	0.67763
			+2.0	1.0	1.0	13.42568
					2.0	5.22914
				2.0	1.0	6.17642
					2.0	1.59155

Figures 2 and 6 show the effect of buoyancy ratio parameter on velocity profiles for H_2O and SO_2 respectively. For aiding effects, the velocity level increases and for opposing effects, the velocity level decreases. Another interesting result is the large distortion in the velocity field caused by decreasing the value of N. Negative values of velocity are predicted in the outer boundary region for opposing effects. This results from incoming flow first experiencing the negative buoyancy effect of thicker species diffusion layer. The flow is eventually drawn upward by the combined action of thermally caused buoyancy and the shear that results there from. These large effects upon the velocity distribution would be expected to have very large effects on the stability of such laminar flows.

It is difficult to define boundary layer thickness exactly. Usually, $y = \delta$ when the boundary layer wall velocity $u(0, t)$ has been decreased by 99% or 99.5% [20]. The values of δ corresponding to these percent decrease in $u(0, t)$ be δ_1 and δ_2, respectively. In order to give a quantitative estimate of the dependence of the boundary layer thickness on the magnetic parameter, we have plotted the boundary layer thickness δ_1 and δ_2 (Figure 3) as function of the time for some typical values of the magnetic parameter. The boundary layer thickness increases with time but magnetic field tends to suppress it. Thus magnetic field has a diminishing effect on the fluid velocity. This fact is also more clearly explained in Figure 4 and Table 1.

Table 2. Variation of skin friction for different parameter.

Pr	Sc	Gr	N	m	t	τ
2.0	23.53	1	-2	1.0	0.1	0.77776
					0.2	1.50943
					0.3	2.26094
				3.0	0.1	1.28604
					0.2	2.77602
					0.3	4.22527
			+2	1.0	0.1	0.39304
					0.2	0.73293
					0.3	1.08725
				3.0	0.1	0.89338
					0.2	1.98110
					0.3	3.01628
7.0	7.0	1	-2	1.0	0.1	0.70174
					0.2	1.39021
					0.3	2.130892
				3.0	0.1	1.230174
					0.2	2.732880
					0.3	4.242094
			+2	1.0	0.1	0.294310
					0.2	0.554817
					0.3	0.847753
				3.0	0.1	0.8062118
					0.2	1.844815
					0.3	2.844930

Figure 4 depicts the variation of velocity with time. For different values of plate velocity the fluid velocity decreases very rapidly near the boundary and its profiles show uniform pattern. Effect of magnetic field also reduces velocity profile. Figure 7 presents the temperature or concentration profiles for different values of Pr or Sc at $t = 0.2$. It is shown that temperature or species concentration profiles at a given point decreases with increasing Pr or Sc.

The skin friction τ at the plate has been given in the Table 2. The results correspond to same saturated liquids (SO_2 and H_2O). The skin friction is proportional to Hartmann number and also increases with time. Aiding effect (*i.e.*

reliable assignments of its vibrational frequencies. A number of modifications over the previous assignments have been made in the present work as a result of normal coordinate calculations for the four probable conformations of this compound.

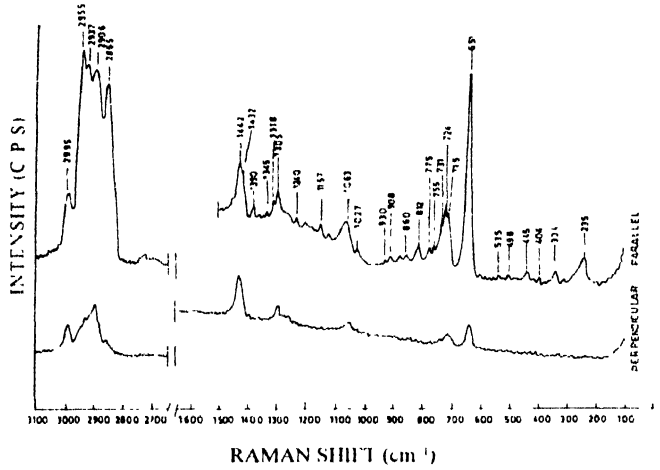

Figure 2. Raman spectra of 1,6-dichlorohexane

The objectives of the present work are to identify the various conformations of 1,6-dicholrohexane present in the liquid phase and its most stable conformer which explains the crystal phase spectrum as well as to make vibrational assignments for all the conformations on the basis of normal coordinate calculations and potential energy (P E.) distribution for each vibrational frequency of the conformers. Also the refined force field of the molecule giving the best fit for the observed frequencies of all the four conformations have been obtained.

2. Calculations

The calculations were made for 1,6-dichlorohexane for its four most probable conformations. Among these the most symmetric conformation has a trans configuration as shown in Figure 3. In this conformation, both the chlorine atoms lie in the C-C skeletal plane of the molecule and it belongs to C_{2h} point group. The other trans configuration is one in which the chlorine atoms lie above and below the skeletal plane with the molecular symmetry C_i. In the third conformation, both the chlorine atoms are on one side of the skeletal plane with molecular symmetry C_2. The fourth conformation has one chlorine atom in the skeletal plane and other above or below this plane and therefore belongs to C_1 symmetry. The normal coordinate calculations were firstly made for the C_{2h} conformation of the molecule by writing its cartesian coordinates, internal coordinates and symmetry coordinates. The force-field used in the present calculations was transferred from the studies of 1-chlorohexane [9]. After refinement of the force-field, it was found that most of the calculated frequencies for the conformer with C_{2h} symmetry fitted well with the prominent bands observed in the crystal phase infrared spectra of the molecule suggesting that this is the most stable conformer of the molecule. The refined force-field was then used to calculate the frequencies of all the four conformers simultaneously along with their separate input data. In the final run nine force constants were put into regression so as to fit sixty observed frequencies with an average frequency error ± 5.4 cm $^{-1}$. The computer program MOLVIB [10] is used in the present calculations. The molecular parameters used in these calculations were C-C = 1.54 Å, C-H = 1.09 Å, C-Cl = 1.77 Å and all the bond angles assumed as 109.47°. The final force constants of the molecule after refinement have been given in Table 1.

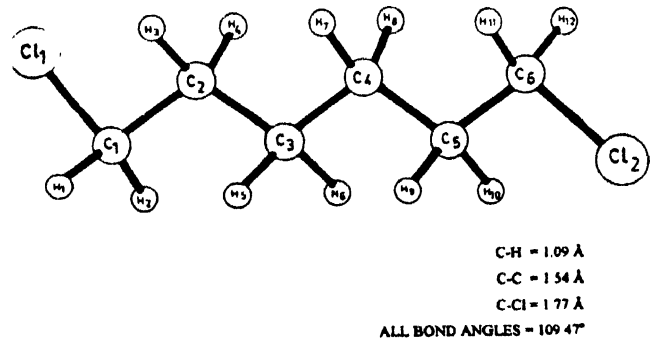

Figure 3. Structure of 1,6-dichlorohexane (C_{2h}).

Table 1. Force constants for 1,6-dichlorohexane

Force constant	Group	Coordinate(s) involved	Atoms(s) common	Value[a]
Strech				
K_r	CH_3	C–H	–	4.792
K_d	CH_2	C–H		4.593
K_R	C–C	C–H	–	4.421
$K_R(Cl)$	C-C-Cl	C–C	-	4.024
K_{Cl}	C–Cl	C–Cl	–	3.560
Stretch-stretch				
F_r	CH_3	CH,CH	C	0.032
F_d	CH_2	CH,CH	C	-0.004
F_R	C-C-C	CC,CC	C	0.238
F_{RCl}	C–C–Cl	CC,CCl	C	0.730
Bend				
H_α	CH_3	HCH	–	0.447
H_β	C–CH_3	CCH	–	0.587
H_δ	CH_2	HCH	–	0.523
H_γ	C–CH_2–C	CCH	–	0.708
H_ζ	C–CH–C	CCH	–	0.708
H_θ	CHCl	ClCH	–	0.697
H_ω	C–C–C	CCC	–	1.331
H_Σ	C–C–Cl	CCCl	–	0.924

Table 1. *(Cont'd)*

Force constant	Group	Coordinate(s) involved	Atoms(s) common	Value[a]
Stretch-bend				
$f_{R\beta}$	C–CH_3	CC,CCH	C–C	0.360
$f_{R\zeta} = F_{R\xi}$	C–CH_2–C	CC,CCH	C–C	0.500
$f'_{R\zeta} = F'_{R\xi}$	C–CH_2–C	CC,CCH	C	0.079
$f_{R\phi} = F_{R\phi}$	C–C–C	CC,CCC	C–C	0.531
$f_{R\Xi}$	C–C–Cl	CC,CCC	C–C	0.075
$f_{\alpha\zeta}$	C–CH_2Cl–C	CCl,CCH	C	0.226
$f_{\alpha\beta}$	CH_2Cl	CCl,ClCH	C–Cl	0.333
$f_{\alpha\phi}$	C–CH_2Cl–C	CCl,CCC	C	–0.220
$f_{\alpha\Xi}$	C–CH_3	CCl,CCCl	C–Cl	0.553
Bend-bend				
$f_{\alpha\alpha}$	C–CH_3	CCH,CCH	C–C	–0.011
f	C–CH_2–C	CCH,CCH	C–C	–0.019
$f_{\alpha\beta} = F_{\zeta}$	C–CH_2–C	CCH,CCH	C–H	–0.054
$f_{\beta\beta}$	CC_3	CCC,CCC	C–C	–0.041
$f_{\beta\phi}$	C–CCl–C	CCCl,CCCl	C–Cl	0.007
$f_{\beta\Xi}$	C–CHCl–C	CCl,ClCH	C–Cl	0.053
$f^t_{\gamma\zeta} = f^t_{\beta\zeta}$	CH_2–CH_2	HCC,CCH [trans]	C–C	0.127
$f^g_{\gamma\zeta} = f^g_{\beta\zeta}$	CH_2–CH_2	HCC,CCH [trans]	C–C	0.047
$f^t_{\gamma\zeta} = f^t_{\beta\zeta}$	C*–CH_2–C*H_2	HCC*,CCH [trans]	C	0.070
$f^g_{\beta\phi} = f^g_{\beta\phi}$	CH_3–C–C–C$(CH_3)_2$	CCC,CCH [gauche]	C–C	–0.043
$f^t_{\omega\phi} = f^t_{\omega\phi}$	C–C–C–CC_2	CCC,CCC [trans]	C–C	0.055
$f^g_{\omega\phi} = f^g_{\omega\phi}$	C–C–C–CC_2	CCC,CCC [gauche]	C–C	0.011
$f^t_{\omega\Xi}$	C–C–C–Cl	CCC,CCCl [trans]	C–C	0.010
$f^g_{\omega\Xi}$	C–C–C–Cl	CCC,CCCl [gauche]	C–C	–0.024
Torsion				
H_τ	C–C	C–C	–	0.009

[a]Stretching constants are in units of mdyn Å^{-1}, stretch-bend constants are in units of mydn Å rad^{-2}.

3. Results and discussion

The conformation I of 1,6-dichlorohexane with C_{2h} symmetry has four symmetry species a_g, b_g, a_u and b_u of vibrational modes. The number of vibrational modes present in each symmetry species are calculated as 16, 11, 12 and 15 respectively with the help of the character table and the well known magic formula. The modes belonging to symmetry species a_g and b_g are active in Raman only and those belonging to a_u and b_u are active in infrared only. For the conformation II which has symmetry C_i each of the vibrational species a_g and a_u has 27 modes which are active in Raman and infrared respectively. In the conformation III with point group C_2, all the vibrational modes are distributed over only two species *a* and *b*. Their number is calculated to be 28 and 26 for species *a* and *b* respectively, are allowed in both the infrared and Raman. The fourth conformation has the symmetry C_1 where all the vibrational modes belonging to only one symmetry species *a* are allowed in both the IR and Raman spectra. A complete assignment of observed bands in the IR (in liquid and crystalline phases) and in Raman for all the four conformations on the basis of the P.E. distributions is presented in Table 2.

Table 2 clearly depicts that while most of the prominent bands of the crystal phase infrared spectra of 1,6-dichlorohexane (Figure 1) were found to correspond to the calculated frequencies of the conformer with C_{2h} symmetry, yet some other relatively weakly observed bands at 1373, 1103, 874, 668, 651 cm^{-1} *etc.* could be correlated to the calculated frequencies for other conformations of the molecule. This shows that the crystal film also contains a small percentage of compound in the amorphous form. As expected, these amorphous phase frequencies are also present in the liquid phase infrared spectra of the compound. All the observed bands of the molecule, whether in the liquid phase infrared (Figure 1) and Raman spectra (Figure 2) or in the crystal film infrared spectra (Figure 1) could be correlated with the calculated frequencies for the above mentioned four conformers belonging to C_{2h}, C_i, C_2 and C_1 symmetries. As already mentioned, the most prominent crystal phase infrared bands have been correlated exclusively with the calculated frequencies of the conformer of symmetry C_{2h}. In addition to the above, two liquid phase infrared bands at 730 and 440 cm^{-1} and two Raman bands at 731 and 498 cm^{-1} also correspond to this conformer only (Table 2). One liquid phase infrared band at 1178 cm^{-1}, besides the crystal phase infrared weak bands at 1160 and 898 cm^{-1} and two Raman bands at 1027 and 755 cm^{-1} correspond to the calculated frequencies of the conformer with C_i symmetry only. Similarly, three crystal phase infrared bands at 1103, 768 and 668 cm^{-1} (which are weak), three liquid phase infrared bands at 1083, 840 and 780 cm^{-1} and five Raman bands at 2906, 1130, 908, 812 and 775 cm^{-1} are correlated only to the C_2 symmetry conformer. Further, crystal phase infrared weak bands at 1373, 1123, 874, 802 and 682 cm^{-1}, liquid phase infrared bands at 1462, 1374, 1346, 1238, 932, 855, 503 and 455 cm^{-1} and Raman bands at 1305, 1240, 930, 745, 724, 445 and 334 cm^{-1} belong to C_1 symmetry conformer only (Table 2).

Table 2. Assignment of observed bands of 1,6-dichlorohexane.

Raman	IR Observed (cm^{-1})		Calculated	P.E.D (%)[a]
	Liquid	Solid	(cm^{-1})	
1,6-Dichlorohexane (C_{2h})				
a_g				
2937 P	–	–	2937	CH_2Clss (99)
2865 P		–	2863	CH_2ss (65)
2865 P	–	–	2870	CH_2ss (65)
–	–	–	1468	$CH_2Cl\omega$ (58)
1442 D	–	–	1442	$CH_2s\delta$ (55), $CH_2s\delta$ (21)
1390 P	–	–	1395	$CH_2s\delta$ (42), $CH_2Cls\delta$ (17), $CH_2s\delta$ (11)
1345 P	–	–	1354	$CH_2Cls\delta$ (48), red. (18), $CH_2s\delta$ (12)
1318 P	–	–	1313	$CH_2\omega$ (71), $CH_2\omega$ (19), CCs (16)
–	–	–	1204	$CH_2\omega$ (62), $CH_2\omega$ (17)
1081 P	–	–	1096	CCss (37), $CCs\delta$ (19), $CH_2Cl\omega$ (18), $CCCs\delta$ (12)
1063 P	–	–	1041	CCss (53), $CH_2\omega$ (11)
–	–	–	958	CCss (62), CCss (22), $CH_2\omega$ (14)
715 P	–	–	715	CClss (89), $CH_2Cl\omega$ (16)
498 P	–	–	493	$CCCs\delta$ (48), $CCCls\delta$ (25)
235 P	–		233	$CCCs\delta$ (63), CClss (14)
–	–	–	160	$CCCls\delta$ (61), $CCC\delta$ (13), $CCC\delta$ (11), CCss (11)
b_g				
2995 D	–	–	2992	CH_2Clas (51)
2955 P		–	2943	CH_2as (76), CH_2as (23)
2937 P	–	–	2936	CH_2as (77), CH_2as (23)
1305 D	–	–	1291	CH_2Clt (54), CH_2t (27)
–	–	–	1195	CH_2t (36), CH_2Clt (23)
–	–	–	1141	CH_2t (94)
–	–	–	1006	CH_2r (38), CH_2r (35), CH_2Clr (19)
860 P	–	–	851	CH_2Clr (48), CH_2r (44)
731 P	–	–	729	CH_2r (55), CH_2Clr (25), CH_2r (14)
–	–		48	$CC\tau$ (64), $CH_2Cl\tau$ (12)
–	–	–	37	$CC\tau$ (34), $CH_2Cl\tau$ (29)
a_u				
–	2990	–	2992	CH_2Clas (48)
	–	–	2946	CH_2as (67), CH_2as (32)
–	–	–	2939	CH_2as (67), CH_2as (32)
–	–	1290	1291	CH_2Clt (56), CH_2t (25)
–	–	1185	1189	CH_2t (39), CH_2t (18)
–	–	1152	1148	CH_2t (84)
–	950	960	946	CH_2Clr (40), CH_2r (38)
–	–	777	777	CH_2Clr (44), CH_2r (26), CH_2r (24)
–	–	700	693	CH_2r (61), CH_2r (28)
–	–	–	102	$CH_2Cl\tau$ (46)
–	–	–	27	$CC\tau$ (69), $CH_2Cl\tau$ (13)
–	–	–	12	$CC\tau$ (47), $CC\tau$ (26), $CH_2Cl\tau$ (18)

Table 2. *(Cont'd).*

Raman	IR Observed (cm^{-1}) Liquid	IR Observed (cm^{-1}) Solid	Calculated (cm^{-1})	P.E.D. (%)[a]
b_u				
-	-	-	2937	CH_2Clss (99)
	2865		2867	CH_2ss (78), CH_2ss (21)
	2865		2860	CH_2ss (79), CH_2ss (21)
-		1468	1469	$CH_2Cl\omega$ (60)
	-	1441	1442	$CH_2a\delta$ (66), red (16)
	-	1420	1420	$CH_2a\delta$ (76), red (19)
-	-	1357	1366	$CH_2Cla\delta$ (64), red (24)
-	-	1255	1269	$CH_2\omega$ (45), $CH_2Cl\omega$ (21), $CH_2Cl\omega$ (20)
		1204	1197	$CH_2\omega$ (76), $CH_2\omega$ (32)
-	-	1049	1057	CCas (47), CCas (41)
	-	1002	993	CCas (57), CCas (33), CCCδ (12)
-	730	730	729	CClas (83), $CH_2Cl\omega$ (14), CCas (14)
	440	-	434	CCCaδ (38), CCCaδ (26), CCas (19), CClas (17)
	-	-	299	CCClaδ (67), CCCaδ (15)
	-	-	73	CCCaδ (53), CCCaδ (31), CCClaδ (18)
Dichlorohexane (C_1)				
a_g				
2995 D		-	2992	CH_2Clas (54)
2955 P	-	-	2946	CH_2as (62), CH_2as (35)
2937 P	-	-	2940	CH_2Clas (54), CH_2as (36)
2937 P	-	-	2934	CH_2Clss (88), CH_2as (10)
2865 P	-	-	2870	CH_2ss (68), CH_2ss (31)
2865 P	-	-	2862	CH_2ss (69), CH_2ss (31)
1442 D	-	-	1447	$CH_2s\delta$ (55), $CH_2s\delta$ (13)
1432 D	-	-	1436	$CH_2Cl\omega$ (58), $CH_2Cls\delta$ (12)
-	-	-	1401	$CH_2s\delta$ (54), $CH_2\omega$ (14)
1345 P	-	-	1354	$CH_2Cls\delta$ (58), red (22)
1318 P	-	-	1319	$CH_2\omega$ (60), $CH_2\omega$ (24), CCss (18)
	-	-	1266	CH_2Clt (39), $CH_2\omega$ (22)
-	-	-	1210	$CH_2\omega$ (50), CH_2t (15), $CH_2\omega$ (10)
-	-	-	1191	CH_2t (61)
1157 P	-	-	1141	CH_2t (91)
1081 P	-	-	1092	CCss (27), CCCsδ (20), CCCsδ (14)
1027 P	-	-	1037	CCss (58)
-	-	-	990	CH_2r (36), CH_2r (29)
-	-	-	973	CCss (57), CH_2r (12)
860 P	-	-	850	CH_2Clr (59), CH_2r (19)
755 P	-	-	762	CH_2r (49), CH_2r (26), CH_2Clr (13)
651 P	-	-	661	CClss (96), $CH_2Cl\omega$ (13)
420 P	-	-	418	CCClsδ (40), CCCsδ (26)
404 P	-	-	398	CCClsδ (56), CCCsδ (16), CCss (13)
-	-	-	201	CCCsδ (26), CCss (16)
-	-	-	41	CCτ (49), $CH_2Cl\tau$ (19)
-	-	-	31	CCτ (47), $CH_2Cl\tau$ (24)

Table 2. *(Cont'd)*

Raman	IR Observed (cm^{-1})		Calculated (cm^{-1})	P.E.D. (%)[a]
	Liquid	Solid		
a_u				
–	2990	–	2992	CH_2Clas (59)
–	–	–	2944	CH_2as (76), CH_2as (19)
–	–	–	2936	CH_2as (68), CH_2Clss (23)
–	–	–	2934	CH_2Clss (72)
–	2865	–	2866	CH_2ss (75), CH_2ss (25)
–	2865	–	2860	CH_2ss (75), CH_2ss (25)
–	1445	–	1446	$CH_2a\delta$ (68), red (18)
–	1432	–	1437	$CH_2Cl\omega$ (63)
–	–	1420	1421	$CH_2a\delta$ (76), red (18)
–	1354	1357	1363	$CH_2Cla\delta$ (50), red. (17)
–	1309	1320	1314	$CH_2\omega$ (36), $CH_2\omega$ (19), $CH_2Cla\delta$ (12)
–	–	1255	1254	$CH_2\omega$ (30), CH_2Clt (16)
–	–	1185	1193	CH_2t (52), $CH_2\omega$ (28), $CH_2\omega$ (15)
–	1178	–	1182	$CH_2\omega$ (39), CH_2t (27), $CH_2\omega$ (13)
–	1158	1160	1151	CH_2t (26)
–	1059	–	1065	CCas (47), CCas (44)
–	985	–	981	CH_2Clr (26), CCas (26), CCCaδ (11)
–	904	898	896	CH_2r (46), CCas (16), CH_2r (14)
–	815	–	821	CH_2Clr (50), CH_2r (17), CCas (13), CH_2Clr (12)
–	–	700	706	CH_2r (72), CH_2t (16), CClas (13)
–	651	651	659	CClas (88), $CH_2Cl\omega$ (12)
–	540	–	541	CCCaδ (41), CCClaδ (15), CCas (12)
–	–	–	260	CCClaδ (67), CCas (16)
–	–	–	153	CCCaδ (61), CCCaδ (22)
–	–	–	81	$CH_2Cl\tau$ (34)
–	–	–	17	Cτ (49), $CH_2Cl\tau$ (24), Cτ (12)
–	–	–	11	Cτ (85)
1,6-Dichlorohexane (C_2)				
a				
2995 D	2990	–	2992	CH_2Clas (55)
2955 P	–	–	2944	CH_2as (75), CH_2as (19)
2937 P	–	–	2936	CH_2as (67), CH_2 Clas (23)
2937 P	–	–	2934	CH_2Clss (72), CH_2as (15), CH_2as (13)
2865 P	2865	–	2870	CH_2ss (68), CH_2as (31)
2865 P	2865	–	2862	CH_2as (69), CH_2as (31)
–	–	1452	1447	$CH_2s\delta$ (55), $CH_2s\delta$ (14)
1432 D	1432	–	1436	$CH_2Cl\omega$ (58), $CH_2Cls\delta$ (12)
–	–	1393	1401	$CH_2s\delta$ (54), $CH_2\omega$ (14)
–	1354	–	1354	$CH_2Cls\delta$ (58), red. (22)
1318 P	–	–	1319	$CH_2\omega$ (24), CCss (19)
–	1278	–	1265	CH_2Clt (56)
–	–	1204	1209	$CH_2\omega$ (53), CH_2t (10)
–	–	1185	1187	CH_2t (72), CH_2Clt (13)

Table 2. *(Cont'd.)*.

Raman	IR Observed (cm^{-1}) Liquid	IR Observed (cm^{-1}) Solid	Calculated (cm^{-1})	P.E.D (%)[a]
1157 D	1158	–	1151	CH_2t (87)
–	1083	1103	1092	CCss (27), CCCsδ (21), CCCsδ (14)
–	1038	–	1037	CCss (59)
–	985	–	977	CCss (72)
908 P	904	–	913	CH_2r (47), CH_2Clr (24)
812 P	815	–	814	CH_2Clr (53), CH_2r (22), CH_2r (11)
715 P	–	–	705	CH_2r (71), CClss (14), CH_2r (13)
651 P	–	651	659	CClss (88), $CH_2Clω$ (12)
420 P	420	–	418	CCClsδ (40), CCCsδ (26)
404 P	–	–	398	CCCsδ (56), CCCsδ (16), CCss (12)
–	–	–	201	CCClsδ (37), CCCsδ (26), $CH_2Clτ$ (11)
–	–	–	80	$CH_2Clτ$ (35)
–	–	–	18	CCτ (50), $CH_2Clτ$ (31)
–	–	–	10	CCτ (95)
b				
2995 D	2990	–	2992	CH_2Clas (55)
–	2960	–	2946	CH_2as (62), CH_2as (35)
2937 P	–	–	2940	CH_2as (54), CH_2as (36)
2906 P	–	–	2934	CH_2Clss (88)
2865 P	2865	–	2866	CH_2ss (75), CH_2ss (24)
2865 P	2865	–	2860	CH_2ss (75), CH_2ss (25)
–	1445	–	1446	$CH_2aδ$ (68), red (18)
–	1432	–	1437	$CH_2Clω$ (63)
–	–	1420	1421	$CH_2aδ$ (76), red (18)
–	–	1357	1363	$CH_2Claδ$ (50), red (19), CH_2Clt (19)
–	1309	–	1314	$CH_2ω$ (35), $CH_2ω$ (18), $CH_2Clsδ$ (11)
–	–	1255	1255	CH_2Clt (48), $CH_2ω$ (30)
–	–	–	1197	CH_2t (61), $CH_2ω$ (14), $CH_2ω$ (11)
–	–	1185	1183	$CH_2ω$ (49), CH_2Clt (24), CH_2t (11)
1130 P	–	1133	1141	CH_2t (92)
1063 P	1059	–	1066	CCas (47), CCas (43)
–	–	1002	1002	CH_2r (25), CH_2Clr (20), CCas (13)
–	950	960	955	CH_2r (26), CCas (25), CCas (24), CH_2r (12)
–	840	–	845	CH_2Clr (51), CCas (20), CCas (13)
775 P	780	768	768	CH_2r (48), CH_2r (29)
–	–	668	662	CClas (97), $CH_2Claδ$ (13)
–	540	–	541	CCCaδ (41), CCClaδ (15), CCCaδ (14), CCas (12)
235 P	–	–	260	CCClaδ (67), CCas (16)
–	–	–	153	CCCaδ (62), CCCaδ (22)
–	–	–	40	CCτ (60), $CH_2Clτ$ (14)
–	–	–	34	CCτ (37), $CH_2Clτ$ (26)
1,6-Dichlorohexane (C_1)				
a				
2995 D	–	–	2992	CH_2Clas (99)
–	2990	–	2992	CH_2Clas (99)

Table 2. *(Cont'd)*

Raman	IR Observed (cm^{-1})		Calculated (cm^{-1})	P E D. (%)[a]
	Liquid	Solid		
2937 P	–	–	2946	CH_2Clas (34), CH_2as (31), CH_2as (20), CH_2as (14)
2937 P	–	–	2943	CH_2as (38), CH_2as (37), CH_2as (15)
2937 P	–	–	2940	CH_2as (34), CH_2as (25), CH_2as (22), CH_2as (12)
2937 P		–	2937	CH_2Clss (99)
2937 P	–	–	2936	CH_2as (40), CH_2as (31), CH_2as (13)
2937 P	–	–	2934	CH_2Clss (78), CH_2as (13)
2865 P	2865	–	2870	CH_2ss (34), CH_2ss (32), CH_2ss (19), CH_2ss (18)
2865 P	2865		2866	CH_2ss (40), CH_2ss (36), CH_2ss (15)
2865 P	2865	–	2862	CH_2ss (36), CH_2ss (31), CH_2ss (20), CH_2ss (12)
2865 P	2865	–	2860	CH_2ss (40), CH_2ss (37), CH_2ss (14)
–	1462	1468	1469	$CH_2Cl\omega$ (16), red (16), $CH_2\omega$ (15)
–	1445	–	1446	$CH_2\delta$ (60)
1442 D	–	1441	1442	$CH_2\delta$ (59)
1432 D	1432	–	1436	$CH_2Cl\omega$ (18), red (16)
–	–	1420	1421	$CH_2\delta$ (44), $CH_2s\delta$ (32)
1390 P	–	1393	1398	$CH_2\delta$ (28), $CH_2\delta$ (20)
–	1374	1373	1365	$CH_2Cl\delta$ (43), $CH_2Cl\delta$ (14)
–	1346		1354	$CH_2Cl\delta$ (43), $CH_2Cl\delta$ (15), $CH_2\omega$ (12)
1318 P	–	–	1318	$CH_2\omega$ (17), CH_2Clt (15), red (27)
1305 D	–	–	1294	CH_2t (27), $CH_2Cl\omega$ (11), red (20)
1305 D	–	–	1291	CH_2r (36), CH_2t (19)
1240 D	1238	–	1256	CH_2Clt (16), CH_2r (14), red (13)
–	–	1204	1207	$CH_2\omega$ (14), red (17)
	–	1185	1196	CH_2t (39), CH_2t (19), CH_2Clt (16), $CH_2\omega$ (12)
–	–	1185	1189	CH_2t (25), $CH_2\omega$ (14), CH_2Clr (17)
–	–	1185	1186	CH_2Clr (30), CH_2t (16), $CH_2Cl\omega$ (12)
–	1158	1152	1150	CH_2t (20), CH_2t (15), CH_2r (13), CH_2r (10)
–	–	1133	1141	CH_2r (28), CH_2r (19), CH_2r (13), CH_2t (11)
–	–	1123	1094	CCs (29), CCs (19), CCs (13)
1063 P	1059	–	1062	CCs (28), CCs (27), CCs (19), CCs (16)
–	1038	–	1039	CCs (40), CCs (17), CCs (17)
	–	1002	1004	CH_2Clt (16), CH_2r (13), CH_2t (12)
–	985	–	986	CCs (31), CCs (18)
–	–	960	963	CCs (44), CCs (21)
930 P	932	–	925	CH_2t (18), CH_2Clt (17), CH_2t (11)
–	855	874	852	CH_2r (22), CH_2Clt (14)
–	–	802	801	CH_2Clr (22), CH_2t (13)
745 P	–	–	738	CH_2r (27), CH_2t (12)
724 P	–	–	721	CCls (84), $CH_2Cl\omega$ (15)
–		682	696	CH_2r (30), CH_2r (20), CH_2r (14)
651 P	651	651	661	CCls (93)
–	503	–	508	CCCδ (30), CCClδ (14)
445 P	455	–	455	CCCδ (32), CCCδ (15)
334 P	–	–	329	CCClδ (31), CCCδ (27)

Table 2. *(Cont'd)*

Raman	IR Observed (cm^{-1}) Liquid	IR Observed (cm^{-1}) Solid	Calculated (cm^{-1})	P E D (%)[a]
235 P	–	–	235	CCClδ (42), CCCδ (22), CCCδ (12)
	–	–	213	CCClδ (27), CCCδ (11), CCτ (12), CCCδ (11)
–	–	–	113	CCτ (29), CCCδ (24), CCClδ (14), CCs (13)
–	–	–	73	$CH_2Cl\tau$ (41), CCCδ (13)
	–	–	45	$CH_2Cl\tau$ (33), CCτ (33), CCτ (12), CCCδ (13)
–	–	–	37	CCτ (31), $CH_2Cl\tau$ (25), CCτ (24)
	–	–	20	CCτ (49), $CH_2Cl\tau$ (19), CCτ (13)
	–	–	14	CCτ (38), CCτ (21), CCτ (19)

[a] Contributions less than 10% are omitted

Abbreviations used as = asymmetric stretch, ss = symmetric stretch, δ = bend, aδ = asymmetric bend, sδ = symmetric bend, ω = wag, t = twist, r = rock, d = redundant; τ = torsion, P = polarized, D = depolarized

There is another feature observed in the infrared spectra of the crystal film of the compound that none of its prominent bands has appeared in the liquid phase Raman spectra of the compound. Such observation was expected whether the crystal film belonged to C_{2h} or C_i symmetry. But C_i symmetry for the crystal film is ruled out since none of the above mentioned prominent bands has been calculated for the a_u species of C_i symmetry of the molecule. Thus, it is concluded that the symmetry in the crystal phase of the compound is C_{2h} and not C_i. This result is also in accordance with the work carried by Sakakibara *et al* [7], where they have confirmed C_{2h} conformer to be present in the crystalline phase of 1,6-dichlorohexane.

A brief discussion of the vibrational frequencies corresponding to various modes appearing in different regions has been given below :

(i) CH-stretch vibrations

The C–H stretch vibrations whether coming from CH_2Cl or CH_2 groups for all the four conformers have been calculated in the frequency range 2992–2860 cm^{-1}, mostly as pure modes (Table 2). Among these the asymmetric vibrations appear with relatively higher values in the order CH_2Cl > CH_2 followed by symmetric C–H vibrations occupying lower positions in the spectra in the same order. These observations are as expected. However, all these calculated frequencies could not find a correlation with the observed bands as the infrared crystal film spectra were recorded in the frequency range 1500–600 cm^{-1} only and the liquid phase infrared spectra show many a broad features of bands. Raman spectra, though show more defined bands in the C–H stretch vibration range, can give only a_g and b_g modes in C_{2h} and a_g mode in C_i symmetry.

(ii) CH_2-group bend frequencies :

The bending vibrational frequencies for the CH_2Cl group present at both the ends of the carbon chain have been calculated in the region 1468–1140 cm^{-1} for CH_2Cl-group symmetric bend, asymmetric bend, wag, twist; CH_2-group bend (symmetric and asymmetric), wag and twist modes. These have appeared mostly as mixed modes in all the four conformations and have been assigned to various observed bands as shown in Table 2

Two CH_2Cl rock and four CH_2 rock modes show intermixing with each other. Only three of these belonging to a_u species in C_{2h} point group are infrared active. Intense crystalline infrared bands at 960, 777 and 700 cm^{-1} corresponding to the calculated bands at 946, 777 and 693 cm^{-1} respectively are assigned in conformation I. These modes have been found to be only slightly sensitive to the conformational changes and have values almost the same as those reported by Sakakibara [6,7] for this molecule.

(iii) CCl-group frequencies :

The two C–Cl stretch vibrations, one symmetric and the other asymmetric, for the conformation I (P_c) with C_{2h} symmetry have been calculated at 715 and 729 cm^{-1}, respectively. Strongly observed Raman band at 715 cm^{-1} and an intense crystalline phase infrared band at 730 cm^{-1} are related to these modes belonging to species a_g and b_u respectively. These values are in the same range as determined for primary halogenated alkanes, namely 710–730 cm^{-1}. This confirms that the molecules with chlorine atoms at both the ends of the carbon chain behave in a way similar to the primary chloro-alkanes [11].

For the conformation II with C_i symmetry, C–Cl symmetric and asymmetric stretch modes have been calculated

within close proximity at 661 and 659 cm $^{-1}$ respectively. A very strongly observed band at 651 cm^{-1} in the liquid phase infrared and Raman spectra both and a weaker band in crystalline phase infrared spectra at 651 cm $^{-1}$ have been correlated to these modes The same values are calculated for the conformation with C_2 symmetry whereas for the conformation with C_1 symmetry the two C–Cl stretch modes have been calculated at 721 and 661 cm $^{-1}$. An intense band observed in Raman spectra at 724 cm $^{-1}$ has been correlated to the calculated frequency at 721 cm $^{-1}$. These calculations are in full agreement with their values for similar molecules reported in the literature [6,11]. This justifies the assumed force-field and structure of the molecule.

CCCl symmetric and asymmetric bend modes have been calculated at 160 and 299 cm $^{-1}$ respectively for conformation I and are within the same range as calculated for 1-chlorohexane [9]. It is evident from the Table 2 that the values for these modes have been calculated at 398 and 260 cm^{-1} for conformation II, at 418 and 260 cm^{-1} for conformation III and at 235 and 213 cm^{-1} for conformation IV as mixed modes. Only a few observed bands in this region could be assigned to these modes.

(iv) CCC-bending frequencies .

For all the four conformations, the CCC bend modes have been calculated within a wide range 541–75 cm $^{-1}$ as mixed modes. This region also gives some conformational sensitive bands as mentioned earlier in this section where the bands assigned uniquely to various conformations have been mentioned.

(v) CC-stretch frequencies .

Five CC stretch modes for conformation I have been calculated at 1096, 1057, 1041, 993 and 958 cm $^{-1}$ as moderately pure modes and the assignment of these bands is shown in Table 2. For the other conformations, these modes are calculated at nearly the same frequencies.

(vi) Torsional frequencies .

The lowest region of the calculated frequencies consist of torsional modes which are pure modes having no interaction with other modes. Since no bands could be observed in the infrared or Raman spectra in this region, the refinement of the torsional force constant could not be made and it was transferred as such from the studies of 2-chloro-4-methylpentane made by Crowder and Jaiswal [12].

4. Conclusions

In the present study of the vibrational spectra of 1,6-dichlorohexane, it could be ascertained that the lowest energy molecular conformation has C_{2h} symmetry as reported earlier [8]. However, the presence of other three conformations of this compound in the liquid phase was predicted earlier only tentatively. The present study has confirmed this prediction as some specific bands have been assigned uniquely to each of these conformations on the basis of normal coordinate calculations. Further, the assignment of a number of bands suggested in the previous study of this molecule has been modified. In the modified assignments include also some of the prominent observed bands namely liquid phase IR bands at 1346, 1238, 1178, 932, 855, 503 and 455 cm^{-1} and Raman bands at 1240, 1081, 731, 715 and 334 cm $^{-1}$ which have been assigned to different vibrational modes in different conformations. Also a few weak crystalline phase IR bands have been assigned to different modes of vibrations for different conformations in the present study which remained unassigned earlier.

The force-field obtained for this molecule as given in Table 1 is quite reliable as the refinement of the force constants have been achieved to fit the calculated frequencies of the molecule with the observed ones within average error of + 5.4 cm $^{-1}$ only.

Acknowledgments

The authors are grateful to Dr. G A Crowder (former Professor, Department of Chemistry, Louisiana Tech University, Ruston, Louisiana, USA) for providing the infrared crystal as well as liquid phase spectra and also the Raman spectra of the compound. He has been courteous to provide us the latest version of the computer program used for the calculations in the present work.

References

[1] W O George, J E Goodfield and W F Maddams *Spectrochim Acta* **41A** 1243 (1985)

[2] Xiabin Jing and S Krimm *Spectrochim Acta* **39A** 251 (1983)

[3] Peter Klaeboe, Claus J Nielsen and David L Powell *Specrochim Acta* **41A** 1315 (1985)

[4] Sung Hyo Chough and Samuel Krimm *Spectrochim Acta* **46A** 1405 (1990)

[5] M S Wu, P C Painter and M M Coleman *Spectrochim Acta* **35A** 823 (1979)

[6] Masaaki Sakakibara, Yoko Yonemura, Zenzo Tanaka, Hiroatsu Matsuura and Hiromu Murata *J Mol Struct* **70** 169 (1981)

[7] Masaaki Sakakibara, Hiroatsu Matsuura and Hiromu Murata *J. Mol Struct* **55** 21 (1979)

[8] R M P Jaiswal, R K Garg and G A Crowder *Proc. Ind. Acad. Sci (Chem Sci)* **102** 661 (1990)

[9] Neena Jaggi and R M P Jaiswal *Indian J Pure Appl. Phys* **38** 69 (2000)

[10] T Sundius *J Mol. Struct* **218** 321 (1990)

[11] Daimay Lin Vein, Norman B Colthup, William G Fateley and Jeanette G Grasselli *The Handbook of Infrared and Raman Characteristic Frequencies of Organic Molecules* (London Academic) (1991)

[12] G A Crowder and R M P Jaiswal *J. Mol Struct.* **99** 93 (1983)